



Secondary Structure Transitions for a Family of Amyloidogenic, Antimicrobial Uperin 3 Peptides in Contact with Sodium Dodecyl Sulfate

Anup K. Prasad^{†, a, b}, Chandni Tiwari^{†, a, c}, Sourav Ray,^{a, b} Stephanie Holden,^[c], David A. Armstrong,^[d] K. Johan Rosengren,^[d] Alison Rodger,^[e] Ajay S. Panwar,^{*[b]} and Lisandra L. Martin^{*[c]}

Secondary structure changes are an inherent part of antimicrobial (AMP) and amyloidogenic peptide activity, especially in close proximity to membranes, and impact the peptides' function and dysfunction roles. The formation, and stability of α -helical components are regarded as essential 'intermediates' for both these functions. To illuminate the conformational transitions leading to amyloid formation we use short cationic AMPs, from an Australian toadlet, *Uperoleia mjobergii*, (Uperin 3 family, U3) and assess the impact on secondary structural elements in the presence of a membrane mimetic surfactant, sodium dodecyl sulfate (SDS). Specifically, Uperin 3.x, where $x=4, 5, 6$ wild-type peptides and position seven variants for each, R7A or K7A, were investigated using a combination of experimental and simulation approaches. In water, U3 peptides remain largely unstructured as random coils, with the addition of salts initiating structural transitions leading to assembly towards amyloid. Solution NMR data show that an unstructured U3.5 wt peptide transitions in the presence of SDS to a well-defined α -helical structure that spans nearly the entire

sequence. Circular dichroism (CD) and ThT fluorescence studies show that all six U3 peptides aggregate in solution, albeit with vastly varying rates, and a dynamic equilibrium between soluble aggregates rich in either α -helices or β -sheets may exist in solution. However, the addition of SDS leads to a rapid disaggregation for all peptides and stabilisation of predominantly α -helical content in all the U3 peptides. Molecular dynamics (MD) simulations show that the adsorption of U3.5 wt/R7A peptides onto the SDS micelle is driven by Coulombic attraction between peptide cationic residues and the negatively charged sulfate head-groups on SDS. Simulating the interactions of various kinds of β -sheet dimers (of both U3.5 wt and its variant U3.5 R7A) with SDS micelles confirmed β -sheet content decreases in the dimers after their attachment to the SDS micelle. Adsorbed peptides interact favourably with the hydrophobic core of the micelle, promoting intramolecular hydrogen bonds leading to stabilisation of the α -helical structure in peptides, and resulting in a corresponding decrease in intermolecular hydrogen bonds responsible for β -sheets.

Introduction

Antimicrobial peptides (AMPs) are a highly diverse group of small proteins (typically <50 amino acids) that are present across all forms of life.^[1] They are typically positively charged and frequently display amphipathic helical structures.^[2] The cationic nature of AMPs facilitates binding to negative bacterial membranes.^[3] AMPs display a broad spectrum of activity against parasites, viruses, fungi, bacteria and other invading pathogens, and as such they form part of the first line of defence against microbes in multicellular organisms.^[4] Due to their wide range of activities and selectivity towards different microbes, AMPs hold potential for the development of new peptide-based antibiotics, an important consideration given the increasing prevalence of microbial resistance to traditional antibiotics.^[3b] Intriguingly, some AMPs have also been shown to form amyloid fibrils whilst some amyloidogenic proteins display antimicrobial properties.^[5] Both amyloidogenic proteins and AMPs have the ability to adopt α -helical structures when in contact with a membrane-like environment, as well as possessing the potential for membrane disruption.^[3a, 4a, 6] It is these similarities that have led to the beguiling hypothesis that amyloidogenic proteins are

[a] A. K. Prasad,[†] C. Tiwari,[†] S. Ray

IITB-Monash Research Academy
Indian Institute of Technology Bombay
Powai, Mumbai-400076 (India)

[b] A. K. Prasad,[†] S. Ray, A. S. Panwar

Department of Metallurgical Engineering and Materials Science
Indian Institute of Technology Bombay
Powai, Mumbai-400076 (India)

E-mail: panwar@iitb.ac.in

[c] C. Tiwari,[†] S. Holden, L. L. Martin

School of Chemistry
Monash University
Clayton, VIC 3800 (Australia)

E-mail: Lisa.Martin@monash.edu

[d] D. A. Armstrong, K. J. Rosengren

School of Biomedical Sciences
The University of Queensland
Brisbane, QLD, 4072 (Australia)

[e] A. Rodger

Department of Molecular Sciences
Macquarie University
Macquarie Park, NSW, 2109 (Australia)

[†] These authors contributed equally to this work.

 Supporting information for this article is available on the WWW under
<https://doi.org/10.1002/cplu.202100408>

 This article is part of a Special Collection celebrating the 10th Anniversary of ChemPlusChem.

aberrant host-defence peptides, which may normally function as a part of the innate immune system.^[7]

The activity of AMPs most often arises from their ability to interact with and disrupt cell membranes. Linear AMPs are typically unstructured (random coil) in solution, undergo a series of conformational changes from a random coil to amphipathic α -helix upon contact with a lipid membrane.^[8] The positively charged surface of the helical peptide binds to the negatively charged bacterial membrane via electrostatic interactions, whilst any hydrophobic region is able to penetrate into the lipid bilayer.^[3a,4c] The way in which the membrane-bound peptide disrupts the lipid bilayer can occur via different routes, including the formation of pores (barrel-stave or toroidal) or a concentration-dependent carpet-like mechanism.^[2b,3a] There are many similarities between AMPs and amyloidogenic peptides in terms of formation of structures as well as their membrane action.^[4a,6b] Notably, self-assembly of the peptides into oligomers is a key factor in membrane disruption, although the required structure (α -helix or β -sheet, morphology and size) is likely to vary.^[4a,5a,9] Thus, it appears that the antimicrobial activity of these peptides depends both on their amyloidogenic properties and ability to permeate cell membranes.

Dermal secretions of amphibians contain an abundance of chemicals involved in host-defence mechanisms, including antimicrobial peptides. Peptides secreted by the dorsal surface of many anurans often display antimicrobial properties, with approximately 200 host-defence peptides isolated from the skin of Australian anurans in the past 25 years.^[10] The uperin family of peptides were isolated from the skin secretions of the Australian toadlet genera *Uperoleia*, and have been shown to have antimicrobial activity, especially towards Gram positive bacteria.^[10b,c,11] Some of the uperin peptides were also found to be membrane active AMPs, with the uperin 3 (U3) members capable of forming fibril structures similar to those formed by amyloidogenic peptides, such as A β in Alzheimer's Disease.^[4a,10b] Interestingly, there is an increasing number of AMPs which can form amyloid like fibrils, such as indolicidin,^[12] magainin 2^[9] and protegrin-1.^[5e] Importantly, we found that the (monomeric) AMP uperin 3.5 (U3.5) is stable in water, and the peptide assembly is initiated upon addition of salts or buffer to the solution.^[4a,13] Thus, U3 family of peptides present ideal candidates to study amyloidogenic mechanisms and antimicrobial activity; and the potential relationship between these two functions.

In our earlier studies we showed that U3.5 (U3.5 wt) and a number of variants,^[13a] as well as U3.x ($x=4, 5, 6$)^[13c] (Table 1) transition through a stable α -helical intermediate(s) on the pathway to stable amyloid structures.^[4a] These amyloid structures were inferred as β -sheet based on physicochemical data including, circular dichroism (CD) and fluorescence through binding to Thioflavin T (ThT) and simulations.^[3a,4a,13c] Not surprisingly, the use of co-solvents, such as trifluoroethanol (TFE) were able to stabilise U3.5 and U3.6^[11] as predominately α -helical structures.^[4a,13a] Intriguingly, recently, Landau *et al.* reported the X-ray structure of a helical cross- α amyloid U3.5, showing that a diversity of secondary structures is possible by modulating the environmental conditions.^[14]

Table 1. Amino acid sequences of the U3 family of peptides under investigation.

	Sequence ^[a]	Charge ^[b]
U3.4 wt	G V G D L I R K A V A A I K N I V –NH ₂	3+
U3.5 wt	G V G D L I R K A V S V I K N I V –NH ₂	3+
U3.6 wt	G V I D A A K K V V N V L K N L F –NH ₂	3+
U3.4 R7A	G V G D L I A K A V A A I K N I V –NH ₂	2+
U3.5 R7A	G V G D L I A K A V S V I K N I V –NH ₂	2+
U3.6 K7A	G V I D A A A K V V N V L K N L F –NH ₂	2+

^[a] Blue and red residues possess a positive and negative charge at physiological pH, respectively (note that the N termini are also positively charged). The 7th position residue is bold. All peptides are C-termini amidated. ^[b] The overall charge at pH 7.40 is shown in the last column.

The antimicrobial activity of the U3 family of peptides was studied by Bowie in 1999,^[11] but of note for this study was that U3.5 and U3.6 showed an almost identical profile towards bacteria, albeit with moderate minimum inhibitory concentration (MIC) values between 3–50 μ g/mL, and most effective towards *Leuconostoc lactis*.^[11] In that same study, they also showed that substitution of positive amino acid residues at position 7 by alanine, removed these antibiotic effects. Subsequently, we correlated this effect for position 7 variants with a much enhanced propensity towards aggregation; in terms of kinetics and amyloid yield.^[3a,13a] To probe further the inverse relationship between amyloidogenic and AMP activities, the influence of phospholipids DMPC, DMPG and cholesterol on the aggregation kinetics showed that negatively charged lipids inhibited U3.5 aggregation stabilising the peptide in a soluble α -helix, as demonstrated by CD.^[13a] Studies using small unilamellar vesicles (SUV) of DOPE:DOPG supported the conclusion that peptide contact with bacterial-mimetic membranes enhanced peptide transition *via* an α -helical secondary structure, although the subsequent evolution into either cross- α or cross- β amyloid polymorphs^[14] was described as chameleon-like varying dramatically with aggregation conditions.

This study aimed to characterise the secondary structural changes of the U3 peptide family in a membrane mimetic environment, using sodium dodecylsulfate (SDS) micelles. The assembly of three U3.x wild type (wt) peptides, U3.4 wt, U3.5 wt and U3.6 wt (sequences shown in Table 1) have been selected for investigation.^[13c,15] Novel variations have been introduced into these U3.x peptides at the seventh amino acid residue position with the intention of reducing the overall positive charge of the peptide from 3+ to 2+, and consequently increasing hydrophobicity, which is expected to enhance the propensity of these peptides to aggregate. These variants are U3.4 R7A, U3.5 R7A and U3.6 K7A. The effect of these position seven variants on secondary structure changes has previously been reported using CD, however, here we have extended the analysis to examine the relative rates and extent of aggregation using ThT fluorescence assay techniques. The NMR structure of the U3.5 wt peptide is reported with SDS micelles and which provides structural information of the secondary structure in this bacterial membrane mimetic environment. Although, it should be noted that an inherent limitation of working with SDS is that it forms small, single layer micelles, unlike lipids that

are capable of forming lipid bilayers thus being good mimics for biological membranes. However, SDS is a useful albeit simplistic membrane mimetic^[16] and our combined experimental (NMR, CD, ThT fluorescence, ATR-FTIR, TEM) and molecular dynamics (MD) simulations approaches were consistent with lipid studies^[13a,14] and those using bacteria.^[10b,11,14] Thus, the overarching purpose of these studies is to investigate underlying secondary structure of normal, soluble peptides into polymorphic assemblies of amyloid, in the presence of bacterial-mimetic surfaces. Our aim is to further our knowledge of the initial molecular events of U3.x peptide structures and their interactions with biomimetic surfaces, thus gain insight as to the functional connection or role of amyloid in antimicrobial peptide function.

Results and Discussion

NMR spectroscopy studies of U3.5 wt in water and SDS micelles

Initially, NMR data were recorded for the U3.5 wt peptide in water at 2.0 mg/ml. These data showed sharp signals, but with very poor dispersion, indicative of a lack of ordered structure (see reference [17] for methods). These data were assigned using sequential assignment strategies based on homonuclear TOCSY and NOESY spectra. $\text{H}\alpha$ secondary shifts, the difference between observed chemical shifts and the equivalent random coil chemical shifts measured in unstructured peptides that sample all possible conformations,^[18] were determined (Figure 1(a)). These secondary shifts were found to be close to zero, confirming that the peptide does not adopt a stable ordered structure but is a dynamic random coil in water.

The addition of SDS (deuterated) resulted in a dramatic change in spectral appearance, with significant improvement in signal dispersion and the appearance of a large number of non-sequential NOEs in the NOESY data, confirming that U3.5 wt interacts with SDS micelles and that this induces an ordered structure.^[17] Resonance assignment and calculation of secondary shift confirmed a structural change, consistent with a helical structure, being observed through most the sequence (Figure 1(a)). Given the high quality of the NMR data and the presence of ordered structure we were able to determine the 3D structure of U3.5 wt in SDS. Interproton distances were derived from cross peak intensities in the NOESY data, and natural abundance HSQC data were used to assign ¹³C and ¹⁵N chemical shifts allowing the determination of backbone dihedral angles using TALOS-N.^[19] Structures were calculated using torsion angle dynamics, which resulted in a well-defined structural ensemble with helical structure throughout most of the sequence (Figure 1(b)). Table S1 summarises the structural and restraints statistics and indicates the structure is of high precision and quality and supported by a large number of experimental constraints. The central helical region extends from residue 4–16 and is highly amphipathic projecting the polar side chains (D4, R7, K8, S11, K14) on one side and the

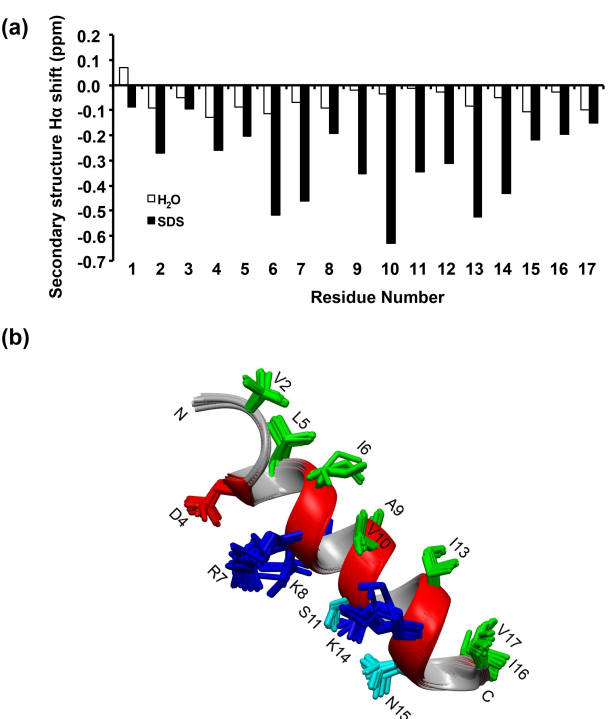


Figure 1. ^1H NMR spectroscopy analysis of U3.5 wt in water and SDS. (a) Comparison of the secondary chemical shifts of the $\text{H}\alpha$ protons for U3.5 amino acids, in water (white) and SDS (black). (b) NMR structure of U3.5 wt following addition of SDS to the solution, showing the final amphipathic α -helical peptide structure.

hydrophobic side chains (V2, L5, I6, A9, V10, V12, I13, I16, V17) on the opposite side.

Circular dichroism and fluorescence studies of U3 peptides

Aggregation properties of U3 peptides

Circular dichroism (CD) data for all six U3 peptides have been previously reported in water and on addition of PBS buffer (0.1 M NaCl, 20 mM phosphate buffer, pH 7.40 \pm 0.02).^[13c] Figure 2(a) illustrates that all six U3 peptides are unstructured (random coil) in water, and that PBS addition initiated structure change, although the kinetics differ significantly with each peptide.^[13c] SOMSpec^[20] was used to devolve the relative contributions of secondary structural (α -helices, β -sheets, turns, bends) and other elements to the CD spectra, in water, and at times 0.0, 1.0 and 24 h after PBS addition (Figure 2(b) and Table S2(a)). Of note, the position seven variants, U3.4 R7A, U3.5 R7A and U3.6 K7A, aggregate faster than the wt peptides and all show increasing α -helical elements over time. Interestingly, U3.5 wt and R7A show the most significant change in β -sheet elements, although this may be in part due to the populations of soluble vs insoluble (microscopic) fractions present in these solutions (see vibrational data below). In accord with dynamic transient helical structure apparent in the MD simulations (see below) it is interesting to note that the U3 peptides always display some CD intensity at ~ 222 nm,^[11,13c] typically character-

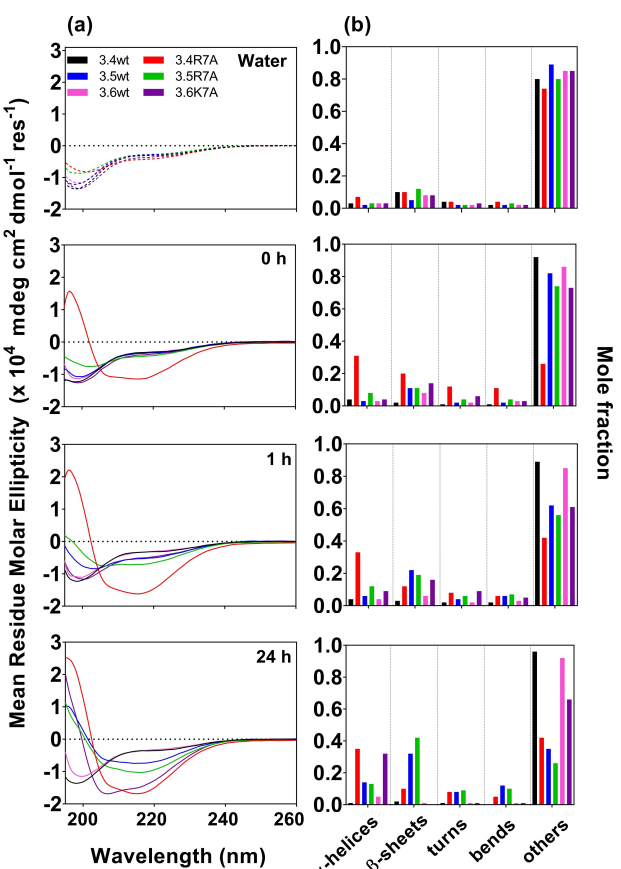


Figure 2. (a) CD spectra for all six U3. x , $x = 4, 5, 6$, wt peptides and their respective R/K7A variants in water and upon addition of PBS at $t = 0, 1, 24$ h at 37°C , and (b) SOMSpec analysis^[20] of secondary structure components.

istic of β -sheet elements. All six U3 peptides exhibit random coil elements in water and these are also present in PBS spectra (Figure 2).

Thioflavin T (ThT) fluorescence, which reports on fibril formation, was used to follow the aggregation process for the six U3 peptides under physiological conditions, typically in PBS at $\text{pH } 7.40 \pm 0.02$. These assays were conducted under quiescent conditions so as to avoid fragmentation events. In each experiment, the U3. x peptides were measured at a concentration of $111 \mu\text{M}$ first in water at a temperature of 37°C . The peptides showed no indication of aggregation for up to 166 h. The addition of PBS initiates fibril formation and results in a final peptide concentration of $100 \mu\text{M}$. As shown in Figure 3, the U3. x peptides all assemble to varying extents; with different initial rates of assembly, as well as maximum amyloid yield. The aggregation curves reveal that each U3. x peptide has a unique kinetic profile, likely due to differences in their microscopic mechanisms underlying fibril formation. However, we note that this technique does not appear to discriminate between β -sheet and α -helical amyloid.^[14,21]

Interaction of peptide aggregates with SDS micelles

The secondary structure of the U3 peptides in an SDS environment was measured using CD and ThT fluorescence. Initially, the change in CD spectra of the six U3 peptides on addition of $10 \mu\text{M}$ SDS to aqueous solutions (measured over 1 h) showed a clear transition from random coil to α -helices as the dominant secondary structure (Figure S1), in each case. No further spectral changes were observed upon addition of PBS to these solutions over 24 h (Figure S1). These results support the U3 peptides as more stable in an α -helical conformation if in a concentrated membrane-mimetic environment. Subsequently, the two fastest U3 aggregators, that also gave a high amyloid yield in ThT fluorescence assays, U3.4 R7A (as shown in Figure 3) and U3.5 R7A^[13a] peptides were allowed to aggregate in a PBS solution at $111 \mu\text{M}$ for 24–26 hr. After this time SDS was added to achieve a final concentration of $100 \mu\text{M}$ (Figure 4, Table S2(b)). In the

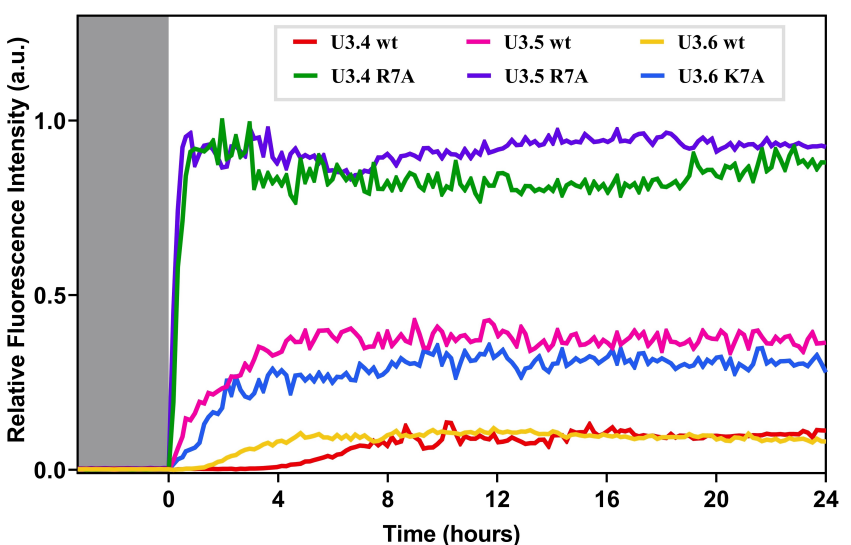


Figure 3. Fluorescence versus time data for the U3. x peptides at $100 \mu\text{M}$. The grey region indicates measurements taken in water prior to the addition of buffer at 0 hours. Data has been normalised to the intensity of the maximum aggregator, as 1.0.

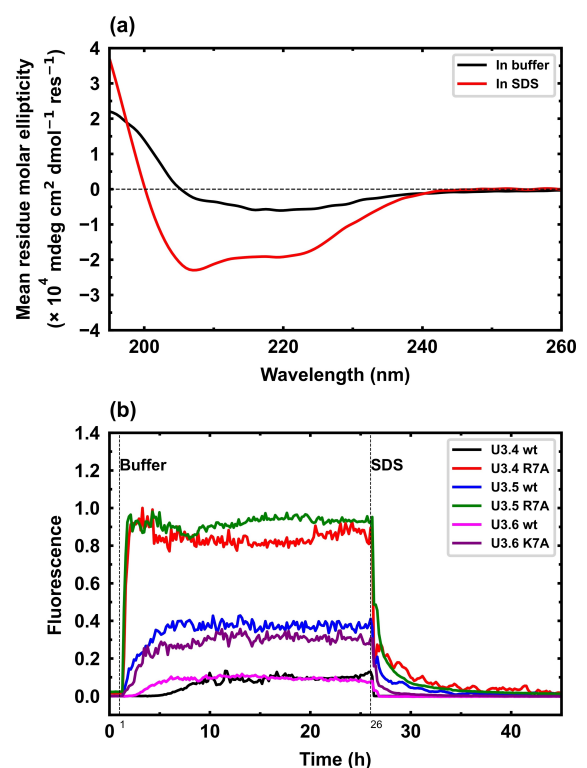


Figure 4. (a) CD spectra for U3.5 R7A indicating a transition from β -sheet to α -helical upon addition of SDS to solution. (b) ThT fluorescence showing aggregation of peptides in PBS solution (at $t = 1$ h) and disaggregation of these aggregates upon addition of SDS to solution at $t = 26$ h.

saline PBS environment, these peptides exhibited negative maximum at ~ 218 nm, characteristic of β -sheet rich content (Figure 4(a)). Deconvolution of these data using SOMSpec^[20] initially ascribed α -helical/ β -sheet content as 15%/38% (U3.4 R7A) and 8%/45% (U3.5 R7A), respectively. Upon addition of SDS to the saline peptide solution, the CD spectra underwent a rapid change to display a minimum (negative maximum) at ~ 208 nm and a broad shoulder around 218 nm, supporting a transition to predominantly α -helical species in solution. SOMSpec^[20] analysis of these spectra in SDS ascribed only α -helical content of 45% (U3.4 R7A) and 50% (U3.5 R7A), respectively, i.e. no β -sheet elements. These effects have been observed previously and are attributed to SDS ‘solvating’ the peptides and thereby disfavouring the intermolecular interactions required for the formation of β -sheet structures.^[16,22] These data suggest that the U3 peptides are likely to be more conformationally stable as α -helical species at membrane surfaces, supporting the notion that the cationic side of the amphipathic α -helix interacts electrostatically with the anionic membrane surface, a key step to membrane disruption for U3.5 wt. This has been previously demonstrated by us^[13a] and Salinas *et al.*^[14] using lipid bilayers or SUVs for U3.5 wt where β -sheet transitions to α -helical secondary structure when SUVs are introduced into solution. We now see it as a more general phenomenon.

ThT fluorescence was used to follow the assembly/disassembly process for the six U3 peptides. As noted above, this

technique does not appear to discriminate between β -sheet and α -helical nature of these aggregates or whether they are soluble protofibrils or amyloids.^[14,21] The U3.x peptides were allowed to reach a maximum fluorescence value in PBS, which is unique for each peptide, as shown in Figure 4(b). Upon addition of SDS to these solutions a rapid reduction in fluorescence when the CD showed formation of α -helical structure. Thus, we are observing the SDS disassembling the amyloid structures for each peptide; with $\sim 50\%$ disassembly occurring over the first hour (Table S3). Thus, the ThT and CD data (Figure 4), support a view of these AMP peptides existing in dynamic equilibrium between monomeric membrane-bound helical structures and amyloid fibres rather than forming irreversible amyloid structures: thus addition of SDS and presumably other membrane environments enables the soluble protofibril populations to access the thermodynamically stable and soluble α -helical state.

Attenuated total reflection Fourier transform infrared (ATR-FTIR) Spectroscopy

The secondary structures of the aggregates were studied using attenuated total reflection Fourier transform infrared (ATR-FTIR) as dried films to ensure we captured all species in the sample (our CD experiments measured only the soluble species). This method can resolve the conformational changes and polymorphism associated with amyloid-prone peptides and proteins,^[23] especially in the diagnostic amide I region ($1620\text{--}1690\text{ cm}^{-1}$). Samples of U3 peptides ($250\text{ }\mu\text{M}$) were first prepared in buffer-free NaCl (0.10 M) and incubated at 37°C for 48 h , centrifugation concentrated the fibril mass that was drop-cast and dried on the crystal and spectra obtained $4000\text{--}800\text{ cm}^{-1}$. All spectra were normalised to 1.0 as the maximum intensity for U3.4 wt at 1658 cm^{-1} . Figure 5 (black trace) shows the amide I band region with either one or two major absorption bands present and these values are reported in Table S4. U3.4 wt and U3.6 wt samples showed only a single band at 1659 cm^{-1} assigned to α -helical structure(s) which was consistent with the ThT fluorescence data (see Figure 3 and 4) and the CD showing these two peptides were the weakest aggregators. The remaining peptides were dominated by an absorption band centred at 1627 cm^{-1} , assigned to β -sheet structure(s) in addition to a band of differing intensities in the α -helical region. In U3.5 wt, these bands were of almost equal intensity, whereas for U3.4 R7A and U3.5 R7A these ratio's were $\sim 1:2$ (α to β) and for U3.6 K7A the ratio was $\sim 1:3$ (α to β). Broadly, these data agree with the ThT fluorescence (see Figure 3 and 4) and CD data (see Figure 2 and 4) reflecting both the propensity of the peptides to assemble into amyloid-rich species and the local secondary structure composition of these aggregates. Only the U3.5 wt ATR-FTIR has been previously reported with the dominant band at 1616 cm^{-1} attributed to cross- β -sheet and a shoulder at 1652 cm^{-1} assigned to α -helical structures, in broad agreement with our data (they prepared their samples by dissolving them in acid, lyophilizing and redissolving at 20 mg/mL before drying whereas we chose

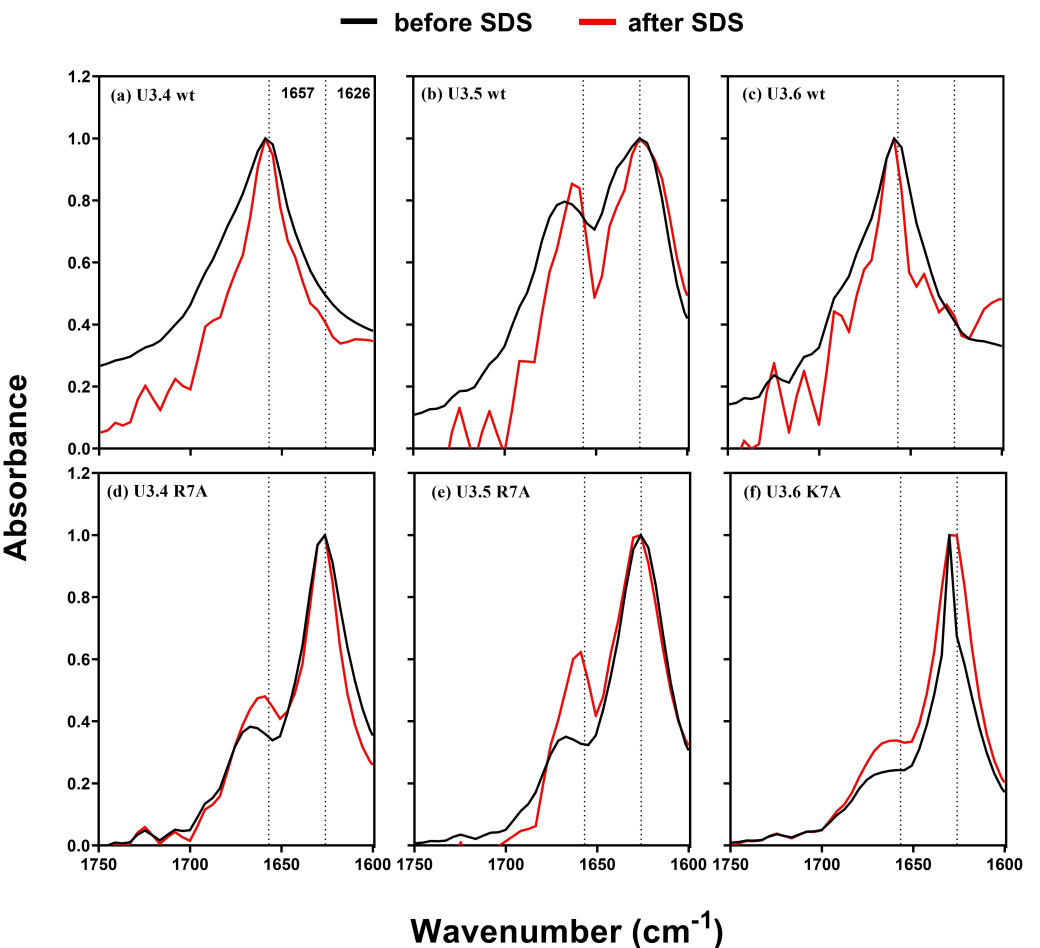


Figure 5. ATR-FTIR spectra of the U3.x peptides normalised to the amplitude of the major amide I band. The black curve corresponds to species resulting from incubation at 37 °C for 48 hours. The red curve samples were prepared in the same manner then, SDS (10 mM) was added and the samples incubated at 37 °C for a further 3 hours and ATR-FTIR measurements were undertaken. All peptides were prepared at 250 μM in 0.10 M NaCl only (no PBS present). The dotted lines represent the major bands for amide I bands of U3.4 wt, assigned to the α -helix and β -sheet absorption modes.

conditions to match the CD and ThT experiments).^[14] Our data compared well with analysis of amyloid- β spectra which were dominated by α -helical (1660 cm^{-1}) and β -sheet (1630 cm^{-1}) structures with the latter more intense in the presence of fibrils.^[23b]

The effect of SDS addition was explored to provide insight into the species present after the disaggregation process observed in the ThT fluorescence data (see Figure 4). The addition of SDS, followed by 3 h further incubation at 37 °C, affected the concentration of peptide on the crystal surface, however the spectra were similar in the overall shapes of the major bands which were normalised to the untreated U3.4 wt sample in Figure 5 (red traces). Despite the sample preparation method enhancing any contribution of amyloid structures, we still note an increase in α -helical content in the presence of SDS. These data are consistent with the SDS micelle interacting with the hydrophobic portion of the helical structure solubilising the aggregates into smaller parcels which would be consistent with the ThT fluorescence and the CD data. One investigation of amyloid- β peptide suggested that ThT fluorescence detected only parallel β -sheets and that anti-

parallel β -sheets attributed to oligomers did not bind to ThT.^[24] We have no evidence of ThT binding preferentially to any fibril. The influence of SDS on fibrils in general has been reviewed albeit with inadequate conclusions.^[23a] What is clear from these data is that the interaction of SDS across the entire aggregation profile of the U3 peptides is complex but does favour disaggregation of β -structures.

Morphology of U3.x peptides by transmission electron microscopy (TEM)

Transmission electron microscopy (TEM) images of the aggregated U3.x peptides was obtained to provide a qualitative visual analysis of each U3 peptide assemblies. For these experiments, the U3.x peptides were prepared at a concentration of 100 μM in PBS and incubated under quiescent conditions at 37 °C for 24 hours, allowing comparisons to be drawn between the CD and fluorescence data. TEM images of the aggregated peptides were captured at similar magnifications to allow comparisons between the size and morphology of the fibrils (Figure 6). All

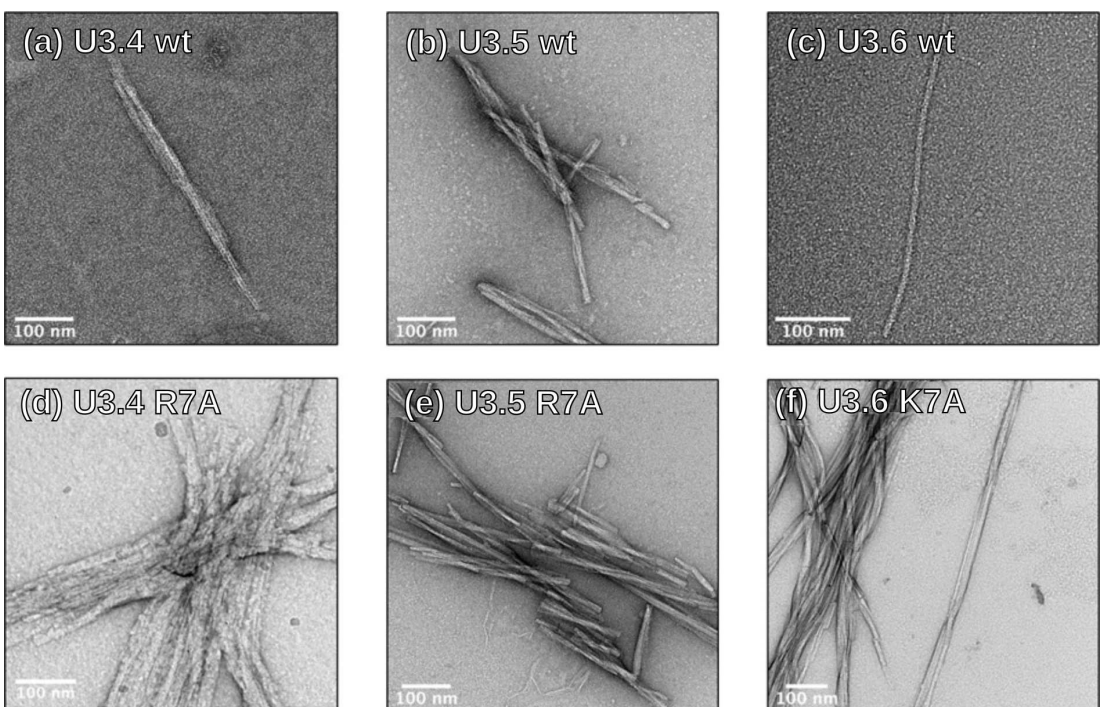


Figure 6. TEM images of the U3.x peptides taken after 24 hours of incubation in a PBS solution at 37 °C. The fibrils were deposited on carbon grids and negatively stained using 2% uranyl acetate. (a)–(c) The U3.x wildtypes. (d)–(f) The U3.x position 7 variants.

peptides exhibited twisted-fibril morphology, albeit showing subtle differences and characteristics including different extents of inter-fibril interactions.

Consistent with the fluorescence data (Figure 3 and 4), representative TEM images for the U3.4 wt and U3.6 wt peptide fibrils were sparse on the carbon grid with U3.4 wt ~540 nm long with a diameter of 33 nm (Figure 6(a)) and those formed by the U3.6 wt peptide, too long to measure and 9.8 nm wide, even more disperse and fewer in number, Figure 6(c). The U3.5 wt peptide frequently displayed twists along the length of the fibril, with a typical example, shown in Figure 6(b) being ~525 nm long and cross-over distance of 82 nm. This is similar to images we have previously reported.^[4a] The three variant peptides all formed extensive fibril mass on the carbon grid, U3.4 R7A peptide formed extensive fibril networks, spanning several mm in size. Closer examination, of the individual fibrils indicated a rough appearance, with nodules protruding from the surface. The U3.5 R7A peptide formed fibrillar aggregates with a width morphologically similar to the U3.5 wt peptide, with a clear twist-like morphology, although these fibrils were straighter and shorter in length than the U3.5 wt (but maintaining a similar width as seen in Figure 6(e) and in our previous report^[4a]). The U3.6 K7A variant formed fibrils that were long with twisted morphology, with the longest observed 5 µm. Similar to the U3.6 wt sample, the U3.6 K7A fibrils were smooth in appearance with an interwoven appearance that resembled ‘braid-like’ structure. The individual fibril (pictured on the right in Figure 6(f)) measured approximately 25 nm in width. The complexity and diversity of amyloid structures has recently been reviewed,^[25] highlighting an extensive range of

polymorphic fibril structures. Together, these TEM images illustrate the typical twisted protofilament morphology that defines amyloid,^[24] although perhaps the exception is U3.6 wt, which could be a single pre-amyloid filament. Previously, we reported Scanning tunnelling microscopy (STM)^[27,28] of the amyloid-β peptide showing the twisted mature amyloid morphology is very similar to that observed for the U3 peptides. Furthermore, our AFM of U3.5 wt peptide are consistent with this morphology observed by TEM.^[4a] To date only U3.5 wt has been structurally characterised using X-ray methods, revealing a ‘dry steric-zipper’ interaction between adjacent peptides generating a cross-α fibril architecture.^[14] Our data suggest the structure is not relevant for our aqueous, PBS and SDS environments.

Molecular dynamics simulations of the U3 peptides

Structure of a single peptide

To understand the atomic nature of the interaction of SDS with the peptides, a single SDS micelle with a U3.5 wt or U3.5 R7A peptide was simulated by allowing the peptide to approach the micelle along a specified direction, as represented by the simulation snapshots shown in Figure 7. Starting configurations for the peptides were extracted from a long (1–2 µs) trajectory simulating a single peptide in aqueous (0.15 M NaCl) solution. Under these conditions, we have previously shown^[13c,24] that a single U3.5 wt peptide adopts largely random coil conformations. Though, partial helical components appeared randomly

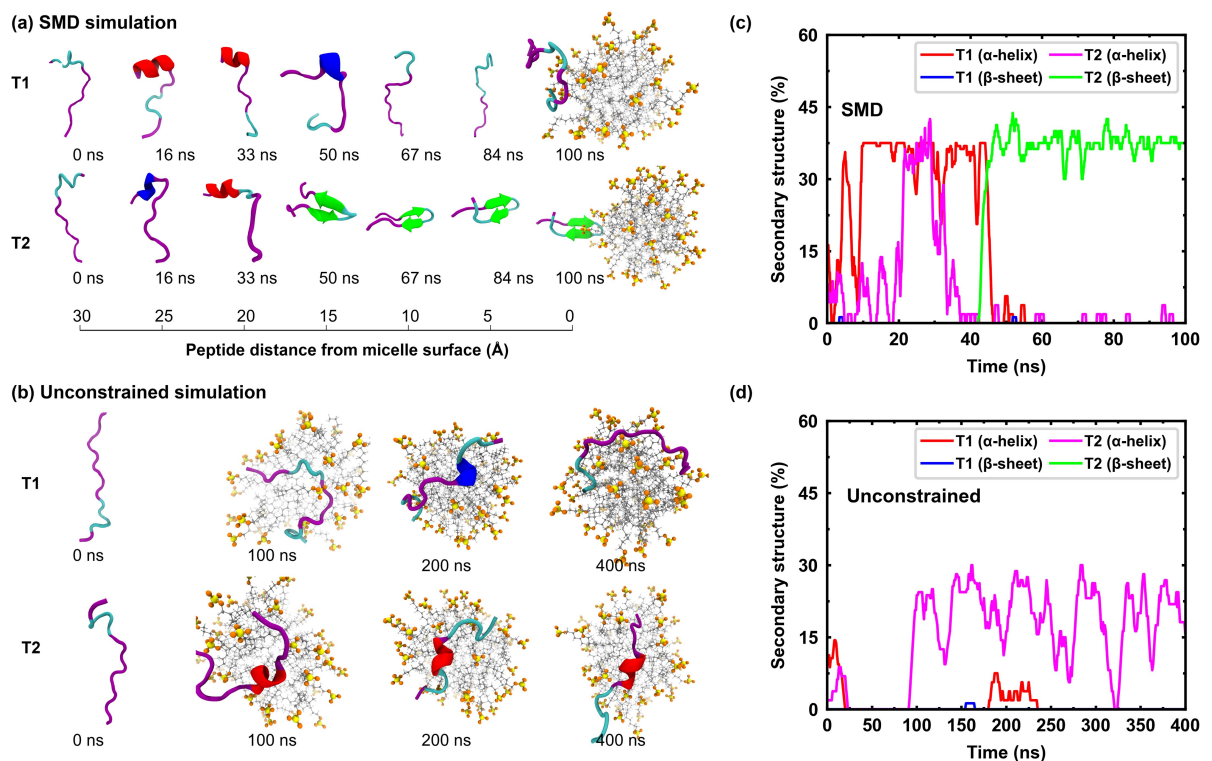


Figure 7. Two trajectories (T_1 , T_2) showing the approach of a single U3.5 wt peptide toward an SDS micelle, using (a) SMD and (b) unconstrained simulations of U3.5 wt peptide's approach toward and attachment onto an SDS micelle in 0.15 M NaCl. Secondary structure evolution for the (c) SMD trajectories and (d) unconstrained simulation trajectories.

at different locations in the peptide sequence, for a single peptide simulation, they were never stable, and the peptide remained unstructured over long durations of time. This is consistent with the NMR measurements (Figure 1) that also confirmed the dominantly random coil structure for U3.5 wt peptide in solution and agreed with the CD measurements of both peptides. The approach of the peptides toward an SDS micelle and its attachment were simulated in two ways; the first involving pulling the peptide with a constant velocity toward the micelle by following a steered molecular dynamics (SMD) simulation scheme (Figure 7(a), Figure S3(a)), and the second where the peptide could move toward the micelle without any constraints (Figure 7(b), Figure S3(b)). In both cases, the centre of mass of the peptide was held fixed at the starting point for a

period of 20 ns to allow for equilibration of ions around the peptide and the micelle. Three statistically independent trajectories were simulated for each of the two simulation setups described above. Two representative trajectories (T_1 and T_2) for each type of simulation are shown in Figure 7 for U3.5 wt. The details of these simulations are listed in Table 2.

All six U3 peptides considered in the current study have similar sequences, with mostly hydrophobic residues and carry either 2+ or 3+ charge. A comparison of the simulated trajectories in Figure 7 (U3.5 wt) and Figure S3 (U3.5 R7A) showed that both U3.5 wt and U3.5 R7A displayed qualitatively similar conformational transitions in their interactions with the SDS micelles. Thus, we focused on understanding the U3.5 wt

Table 2. Details of the MD simulations.

Simulation [box volume in \AA^3]	Simulation type	Initial distance from micelle surface [\AA]	Total no. of atoms	Simulation time [ns]
U3.5 wt monomer-micelle ($150 \times 90 \times 90$)	SMD	35	115296	100
U3.5 R7A monomer-micelle ($150 \times 90 \times 90$)	Unconstrained	35	115296	450
U3.5 wt dimer-micelle ($130 \times 90 \times 90$)	SMD	35	115296	100
U3.5 R7A dimer-micelle ($130 \times 90 \times 90$)	Unconstrained	35	115296	450
U3.5 wt monomer-micelle ($130 \times 90 \times 90$)	Alpha-helix	20	99634	750–1000
U3.5 R7A monomer-micelle ($130 \times 90 \times 90$)	Parallel beta sheet	20	99592	750–1000
U3.5 wt monomer-micelle ($130 \times 90 \times 90$)	Antiparallel beta sheet	20	99616	750–1000
U3.5 R7A monomer-micelle ($130 \times 90 \times 90$)	Parallel beta sheet	20	99539	750–1000
U3.5 R7A monomer-micelle ($130 \times 90 \times 90$)	Antiparallel beta sheet	20	99539	750–1000
U3.x monomer-micelle ($65 \times 65 \times 65$)	Helical simulation	0	22000–24000	40

peptide as a model peptide to describe the U3.x peptide-SDS micelle interactions.

For the SMD runs, the U3.5 wt peptide started at a separation distance, $d = 35 \text{ \AA}$ away from the surface of the micelle and was pulled toward the micelle with a constant velocity of 0.3 \AA/ns . Given the small pulling velocity, the distance was traversed in a span of 100 ns and the peptide's approach toward the micelle approximated a quasi-static process, where the peptide passed through a series of equilibrium states toward the micelle. In this way, SMD simulations described evolution of the peptide conformation as a function of its distance from the micelle surface. When all constraints were removed in unconstrained MD simulations, the peptide accelerated rapidly toward the micelle surface due to a strong peptide-micelle electrostatic attraction (Figure 7(d)). The rapid movement of the peptide made it difficult to systematically assess changes in peptide conformation as a function of peptide-micelle separation. Hence, the need for the SMD simulations. Any helical content that appeared in the peptide during its initial approach, disappeared at $d = 15 \text{ \AA}$ from the micelle surface ($T1$ and $T2$ SMD trajectories are shown in Figure 7(c) and the peptide adopted configurations in the form of either elongated coils or β -strand. Ultimately, the peptide adsorbed onto the micellar surface due to electrostatic attraction between its cationic residues and the anionic SDS head groups with little or no secondary structure. The long-range nature of electrostatic interactions leads to unwinding of any partial helical structure in the peptide at a significant distance from the surface. A plot of the electrostatic energy contribution to the peptide-micelle interaction in Figure S4(b) confirms that Coulombic attraction is dominant for $d < 20 \text{ \AA}$. Significantly, the helical unwinding and subsequent elongation of the peptide occurred at $d \approx 15 \text{ \AA}$. Figure S4 also shows peptide-micelle energetic interactions for the cases of both U3.5 wt and U3.5 R7A are very similar. The electrostatic energy contributions are somewhat lower for U3.5 R7A because it carries one less positive charge in comparison to U3.5 wt. To confirm the constraining of these simulations was not affecting the secondary structure, the peptides were again positioned at a starting distance of $d = 35 \text{ \AA}$ and allowed to evolve without a pulling force (Figure 7(b)). The peptides rapidly moved toward the micelle solely under the influence of attractive electrostatic interactions, losing its entire helical content at $d \approx 20 \text{ \AA}$ consistent with the SMD simulations (Figure 7(d)). Adsorption of the peptide onto the SDS micelle occurred in less than 100 ns (see Figure S5(a)). The unconstrained U3.5 wt simulations were extended to 400 ns to observe possible changes in peptide secondary structure after its adsorption. Structural changes in the adsorbed U3.5 wt peptide were observed as early as 100 ns with one trajectory ($T2$ in Figure 7(d)) showing a massive increase in α -helical content from zero to nearly 25% in a span of 10 ns . The peptide in this trajectory retained its helical content for the rest of the simulation period indicating that the micelle-U3.5 wt interaction stabilised the helical content in the peptide. A corresponding increase in the number of hydrogen bonds within the peptide was observed for this trajectory (see Figures S5(b) and (d)). Further, the peptide orientation on the

micelle surface evolved over time to align its hydrophobic residues with the hydrophobic core of the micelle, consistent with the amphipathic nature of U3.5 wt peptide (see Figure S6). Analysis of the peptide-micelle interaction energy data in Figure S5(c) not only shows a very large decrease in the electrostatic energy due to Coulomb attraction, but also a significant decrease in the van der Waals (vdW) energy upon adsorption of the peptide onto the SDS micelle. This strongly suggests that the SDS micelle stabilises the α -helical structure in an adsorbed U3.5 wt peptide by promoting intra-peptide residue-residue interactions. The $T1$ trajectory also showed an emergence of helical structure around 175 ns , which was retained for nearly 50 ns before the peptide unwound back into an extended coil conformation. The differences between the two simulations illustrates the distribution of structures in a molecular sample. Significantly, β -sheet components were absent throughout the simulation period for both cases.

Simulation of U3 peptide dimers with SDS micelles

To simulate the effect of SDS on U3 aggregates, we introduced dimeric aggregates in the simulation box and placed them at $d = 20 \text{ \AA}$ from the micelle surface. This distance was based on the value of $\kappa^{-1} \approx 0.8 \text{ nm}$, consistent with observations of the peptide accelerating toward the micelle for $d < 20 \text{ \AA}$ in the single peptide simulations (see Figure S5(a)). Dimeric aggregates were again sampled from $2.5 \mu\text{s}$ long 20 mM multi-peptide simulation trajectories of U3.5 wt and U3.5 R7A (see Figure S7). For both peptides, simulation trajectories were monitored for stable dimeric aggregates of the following three types: (i) an α -helical dimer, (ii) a parallel β -sheet dimer, and (iii) an anti-parallel β -sheet dimer. Upon sampling the dimer configurations, five simulations were setup for both U3.5 wt and U3.5 R7A, including three dimer types for U3.5 wt (α -helical, parallel β -sheet and anti-parallel β -sheet dimers) and two dimer types for U3.5 R7A (parallel β -sheet and anti-parallel β -sheet), respectively. These starting configurations are represented by simulation snapshots at $t = 0 \text{ ns}$ in Figure 8(a). For every trajectory, the system was equilibrated for an initial period of 50 ns by holding the dimer centre of mass fixed at its starting position, following which the dimer could move toward the SDS micelle without any constraints. Each trajectory was simulated for a minimum of 750 ns . Trajectories for both U3.5 wt and U3.5 R7A anti-parallel β -sheet dimers were extended to $1 \mu\text{s}$ (see Figure S8).

The findings of the dimer simulations were very interesting, with all five dimers rapidly adsorbing onto the micellar surface in less than 50 ns (see Figure S9; peptide-micelle distance). Despite the reduced charge of the U3.5 R7A variant relative to the wt, there was no qualitative difference between the U3.5 wt and R7A peptides' approaches toward the micelle. Although, the α -helical U3.5 wt dimer disintegrated into peptide monomers by 150 ns , it did not show any significant decrease in its α -helical content. Throughout the simulation period, individual peptides stayed adsorbed on the micelle surface but moved apart from each other over time. It is known that U3.5 wt forms

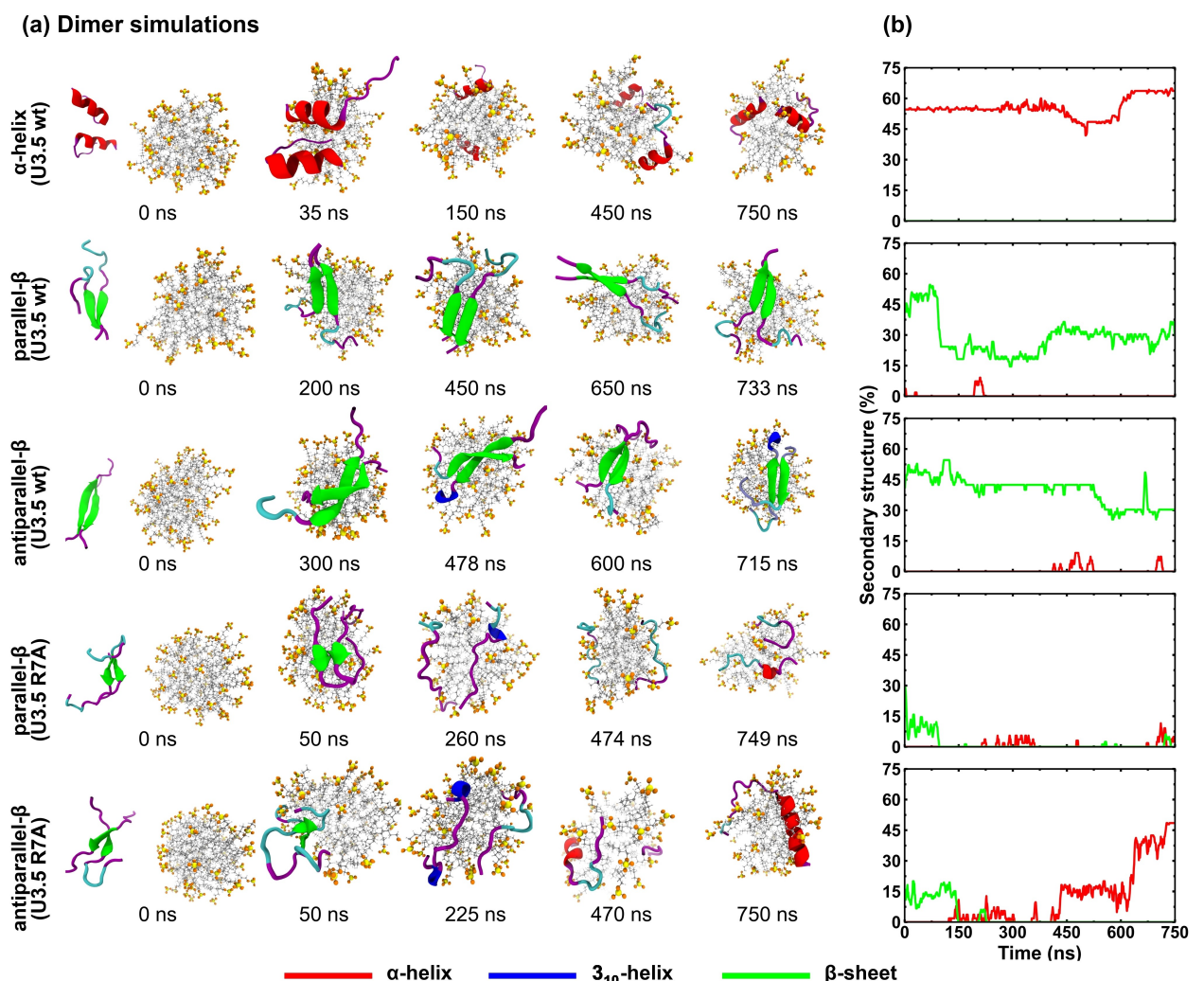


Figure 8. (a) Representative simulation snapshots showing the adsorption of different dimer of U3.5 wt (top three rows) and U3.5 R7A (bottom two rows). (b) Evolution of α -helical and β -sheet secondary structure components for five dimers.

amphipathic helices which can lead to the formation of stable α -helical aggregates^[14] where the helices are held together via hydrophobic interactions between their residues. The disintegration of the dimer into its constituent monomers on the SDS surface indicates that the interaction of the peptide hydrophobic residues with the hydrophobic core of the micelle leads to a lowering of the free energy for the system (Figure S9(a)). When the peptides adopt amphipathic helical conformations, it becomes easier for the hydrophobic residues to align favourably with the hydrophobic core of the micelle. No change in the number of intra-peptide hydrogen bonds was observed (see Figure S9), and the helical peptides appeared to insert themselves into the hydrophobic core of the micelle. The insertion can be inferred from the large negative values of the micelle-peptide distance in Figure S9. This is a significant result since it shows that the α -helical conformation of the U3.5 wt is favoured on the micelle surface. In fact, the overall α -helical content increased by nearly 10% toward the end of the 750 ns simulation (see Figure 8(b)). In contrast to the α -helical dimeric form, a loss of the starting secondary structure was observed

for the parallel and antiparallel β -sheet dimers for both U3.5 wt and U3.5 R7A. The β -sheet content decreased after attachment of dimers to the micelle in all four cases, consistent with our CD measurements (Figures 2, 4 and S1) and with results of Salinas *et al.*^[14]. As expected, the number of hydrogen bonds in the β -sheets, estimated by the inter-peptide hydrogen bonds in Figure S9, showed a corresponding decrease after attachment of the parallel and antiparallel β -sheet dimers.

The extent of loss in β -sheet content differed for every case (Figure 8(b)), depending on the stability of the β -sheet dimer. Whereas, the parallel β -sheet U3.5 wt dimer showed a large 30% decrease in β -sheet content immediately after attachment, antiparallel β -sheet U3.5 wt dimer showed a much lower decrease of 10%. This is expected because anti-parallel β -sheets are more stable in comparison to parallel β -sheets. Similarly, the rate of loss of β -sheet content for the antiparallel β -sheet U3.5 wt dimer was slower compared to the parallel β -sheet U3.5 wt dimer. In both cases, the appearance of small amounts of short-lived α -helical structure was observed. Initially, these structures were not sustained over time. Rather, they appeared to be

unsuccessful nucleation events for α -helices. We speculated that over time they would result in stable nuclei were an experimental-timescale simulation feasible. Indeed, this turned out to be the case when the antiparallel β -sheet U3.5 wt dimer simulation was extended to 1 μ s, where stable α -helical content (~8%) was observed after 900 ns (Figure S8(a)).

Similar trends of decreasing β -sheet contents were observed for parallel and antiparallel β -sheet dimers of U3.5 R7A. Interestingly, a transition to a stable α -helical structure was observed for the antiparallel β -sheet dimer of U3.5 R7A during the later stages of the simulation (Figure 8(b)). The total α -helical content increased to nearly 50% by 700 ns and retained that value for the remainder of the 1 μ s simulation (Figure S8(b)). A U3.5 R7A peptide with prominent α -helical content can be seen very clearly in the 750 ns snapshot in Figure 8(a) for the antiparallel β -sheet dimer. The transition to predominantly α -helical conformations was like the transition observed in unconstrained simulations of single U3.5 wt peptides. This was accompanied with a decrease in inter-peptide hydrogen bonds and increase in the number of intra-peptide hydrogen bonds that promoted stable α -helical peptide conformations (Figure S9(b)). Lower initial β -sheet contents in the U3.5 R7A dimers, indicative of less stable β -sheets, could be reasons why these two trends were captured in the case of U3.5 R7A and not for the U3.5 wt dimers. The transition to stable α -helical structures was most convincingly demonstrated for antiparallel β -sheet U3.5 R7A dimers where stable α -helices with very high α -helical content (~50%) were observed on the micelle surface (Figures 8 and S8(b)). In their experiments, Salinas *et al.*^[14] showed that thin films of U3.5 wt, composed largely of β -rich fibrils, transitioned to α -helical conformations upon addition of SUVs. Thus, our simulations show that the SDS micelle, a bacterial membrane mimic, can alter both peptide-peptide and residue-residue interactions in ways that stabilise α -helical structure in the peptide on the surface of the micelle (*the reader is also referred to simulation movies M1_U3.5wt_parallel and M1_U3.5R7A_antiparallel in the Supporting Information*).

Simulation of peptide-micelle interactions

Based on our experiments and simulations in the current work and experimental data from Salinas *et al.*^[14], it is clear SDS micelles promote the stabilisation of α -helical structure of U3 peptides. Sequence-spanning stable U3.x wt α -helical conformations on SDS surfaces at steady-state in contact with SDS micelles were therefore simulated. The starting structure for U3.5 wt was based on the α -helical representation determined by NMR for aqueous SDS detergent. (It should be noted that no definite peptide structure could be obtained in a solely aqueous environment.) Using SWISS-MODEL Workspace,^[30] the initial structure of U3.4 wt was generated using the U3.5 wt as a template. These two peptides differ by only two amino acids of their sequences at the eleventh and twelfth positions, as indicated in Table 1, so it is not surprising that U3.4 wt also has an α -helical secondary structure. An α -helical structure was also

imposed on the U3.6 wt peptide sequence, using the Protein Builder module^[31] available in VMD.^[32] (The U3.6 wt peptide has been shown to adopt a predominantly α -helical amphipathic structure by NMR in the membrane-mimicking TFE-aqueous environment^[11] despite its low aqueous helical content by CD in this work.) In order to generate an alanine variant of the three U3.x wt peptides, the Mutator plugin of VMD was employed to execute a point substitution at the seventh-position of the wild-type peptides. Hence, like their wild-type templates, these three variants were also primarily α -helical at the onset of the respective simulations. For every peptide, a U3.x peptide was docked with the SDS micelle to prepare a starting structure for a 40 ns long MD simulation to calculate peptide-micelle interactions.

The electrostatic and vdW energy contributions to the net non-bonded interaction energy were obtained for every U3 peptide as time-averaged values of individual contributions over the last 20 ns of their respective simulations (Figure 9). The large negative electrostatic energy component overwhelmed the vdW component for all U3 peptides and emerged as the primary determinant of the total non-bonded interactions (sum of electrostatic and vdW interactions). Plots of interaction energies of only the seventh-position (R/K7) residues with SDS micelles show (Figure 9(b)) that the difference between interaction energies between a U3.x wt peptide and its variant (Figure 9(a)) can be attributed to the loss of the electrostatic interaction energy between R/K at the seventh position and the SDS micelle (Figure 9(b)). Though, the peptide-micelle electrostatic interaction energy values were lower in magnitude (by around 100–200 kcal/mol) for the variants when compared to

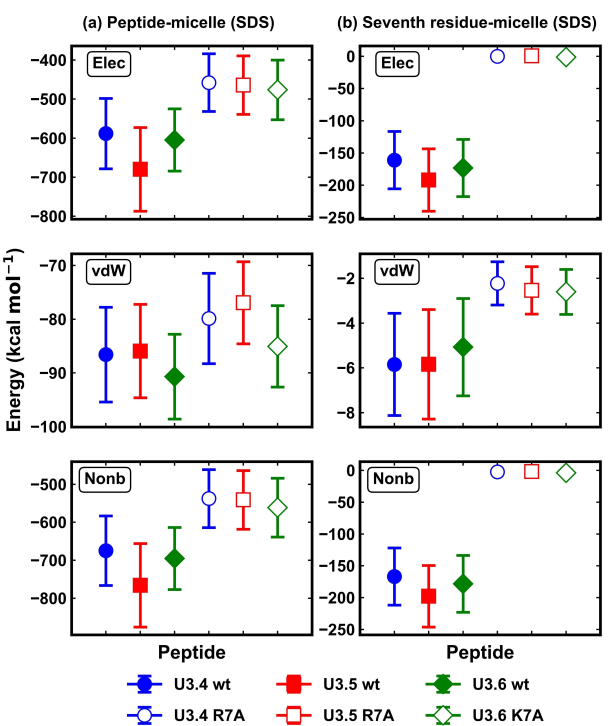


Figure 9. Interaction energies: electrostatic, vdW and total non-bonded for U3 family of peptides, (a) U3.x, $x=4, 5, 6$, wt and (b) seventh-position R/K7A variants with SDS micelles.

the wild type peptides, the total interaction energy values for all six U3 peptides remained large negatives for all U3 peptides. Thus, large, attractive non-bonded energy components show peptide α -helical conformations are stabilized on the SDS surface, and this is primarily driven by Coulombic attractions between cationic peptide residues and sulfate groups of SDS. The effects of this strong peptide-micelle interaction on the peptide behaviour in association with the SDS micelle are discussed in the SI (see Figures S10–S12).

Conclusion

The U3 family of peptides are AMPs, and AMPs are known to adopt helical conformations in membranes. However, the U3 peptides were known to have complex structural profiles depending on conditions. In this work we have explored how different environments (water, salt, buffer, detergent) affect the structures of three wild type and three reduced charge variants U3 peptides. We have found using NMR, CD, and simulations that the bacterial membrane mimetic SDS micelles induces a coil-to-helix transition in an adsorbed U3.5 wt consistent with the role of membrane-peptide interactions imparting a functional structure to the AMP. Structural transitions in U3 peptides interacting with SDS micelles (bacterial membrane mimic) were explored using a combination of experimental and simulation tools. Secondary structure transitions observed in presence of the membrane mimetic provides a crucial link between their inherent amyloidogenicity and their membrane-disrupting antimicrobial activity. Intriguingly, the micelles readily reversed even the formation of salt-induced stable amyloid-structures. In aqueous solution, single U3.5 wt peptides remain largely unstructured, in the form of random coils, and adsorb onto SDS micelles due to Coulombic attraction between their cationic residues and the negatively charged sulfate head-groups on SDS. NMR data show that an unstructured U3.5 wt peptide transitions in presence of SDS to a well-defined α -helical structure that spans nearly the entire sequence. MD simulations confirm that peptide interactions with the hydrophobic core of the SDS micelle stabilise an α -helical structure in the peptide by promoting residue-residue hydrogen bonds within the peptide. Both CD and ThT fluorescence studies show that all six U3 peptides aggregate in solution, albeit with vastly varying rates, and a dynamic equilibrium between soluble aggregates rich in either α -helices or β -sheets may exist in solution. However, the addition of SDS leads to a rapid disaggregation in all peptides and stabilisation of predominantly α -helical content in all the U3 peptides. Simulating the interactions of various kinds of β -sheet dimers (of both U3.5 wt and its variant U3.5 R7A) with SDS micelles confirmed β -sheet content decreases in the dimers after their attachment to the SDS micelle. More importantly, this decrease is accompanied by a corresponding decrease in peptide-peptide hydrogen bonds and a concomitant increase in the intra-peptide (residue-residue) hydrogen bonds responsible for stabilisation of the α -helical structure in the peptide.

All α -helical forms of the six U3 peptides adopt amphipathic conformations with a hydrophobic and hydrophilic side which enable insertion (at least in part) of peptides into the hydrophobic core of the micelle. Simulations of interactions of all α -helical U3 peptide sequences with an SDS molecule show that, though all peptides adsorb onto the SDS micelles due to Coulombic interactions, the alanine substituted U3.x R/K7A variants have a weaker interaction with the micelle when compared to their wild-type counterparts. As position 7 is on the hydrophilic side of the α -helical peptides (Figure S6), this points to significant complexity in membrane-peptide interactions perhaps relating not only to membrane-peptide interactions but also to the different solubilities of the helices in aqueous solution (variants are less prone to forming helices in water than the wt peptides). In our earlier work^[13c] with the same set of the six U3.x peptides we have shown an inverse relation between the α -helical stability of single peptides in solution and their amyloidogenic propensity. The results of the current work point to the crucial role of structural transitions in determining the interactions of amyloidogenic U3 peptides with membrane-mimic SDS micelles. Such structural transitions may be key to understanding the link between their amyloidogenic propensity and antimicrobial activity.

Experimental Methods

Materials

Phosphate buffered saline (0.1 M NaCl + 20 mM phosphate, PBS) was prepared using potassium phosphate monobasic (KH_2PO_4 , anhydrous 99%) and potassium phosphate dibasic (K_2HPO_4 , anhydrous) purchased from Sigma-Aldrich (St. Louis, USA) and sodium chloride (NaCl) from Merck (Darmstadt, Germany). The pH of the buffer was adjusted to 7.4 using sodium hydroxide (NaOH), Ajax Finechem (New South Wales, Australia), and hydrochloric acid (HCl), Sigma-Aldrich (St. Louis, USA). All solutions were prepared using filtered and UV-treated ultrapure water with a resistivity of 18.2 M Ω ·cm (Sartorius AG, Gottingen, Germany).

Peptide synthesis

The U3.x peptides were purchased from Peptide 2.0 (Virginia, USA) and recorded to be at least 99.15% purity; however, for the NMR study, U3.5 wt was assembled in house on Rink amide resin (0.45 mmol/g loading) using standard Fmoc chemistry with HBTU/DIEA activation on an CS336X automated peptide synthesizer (CS Bio). All coupling reactions were performed with 4 equiv. (relative to resin loading) of Fmoc-Amino acid/PEG-OH, 8 equiv. of HBTU, and 8 equiv. of DIEA. After peptide synthesis the N-terminal Fmoc group was removed by addition of 20% piperidine in DMF (2 × 5 min). The completed peptide was cleaved from the resin with TFA/TIPS/Milli Q (95:2.5:2.5) and lyophilized. The crude peptide was dissolved in 10% acetonitrile and purified by RP-HPLC on a Prominence HPLC system (Shimadzu) using a semi-preparative Grace Vydac C18 column (250 mm × 10 mm, 10 μm) with a 1% gradient of buffer A (0.05% TFA) and buffer B (90% acetonitrile, 0.05% TFA) and a flow rate of 3 ml/min. Analytical RP-HPLC and electrospray mass spectrometry (API2000, AB Sciex) was used to verify the purity and molecular weight of the peptide. Theoretical

mass for UU3.5 wt is 1780.16 g/mol, and the observed mass was 1779.2 g/mol, with a purity of ~100%.

Circular Dichroism

All buffer solutions, peptides stock solutions and solutions for CD studies were prepared identically to those previously reported by us.^[13c]

SDS samples: A 100 mM stock solution of SDS was prepared in water and filtered through a 0.2 µm hydrophilic polypropylene membrane filter (Pall Life Sciences, New York, USA). This was stored at room temperature for a maximum of two weeks. The peptides were measured in water and 11.11 mM SDS prior to the addition of PBS, lowering the SDS concentration to the required concentration (~10 mM). CD measurements were conducted hourly for 24 h at 37 °C. The required volume of water was delivered directly to the cuvette, followed by the appropriate volume of PBS and peptide stock. The cuvette was inverted ten times to ensure thorough mixing, prior to placement in the instrument holder. All CD spectra were recorded from 260 to 180 nm at a temperature of 37 °C.

SOMSpec analysis: The self-organising map SOMSpec analysis to CD structure fitting has been described in detail elsewhere.^[20a] It essentially involves moving spectra of a reference set into locations of similar spectral shape on a 2-dimensional map than then placing an unknown in the best place on the map. The secondary structure of the map is determined to be that of its best matching node which in turn is derived as a weighted sum of the secondary structures of the nearest neighbour reference spectra on the map. Protein structure fitting using a reference set of globular proteins does not work well for peptides, so we followed our recent work where we first remove different amounts of random coil CD intensity and perform the structure fitting on those spectra.^[20b] In general the percentage derandomisation with the smallest normalised root mean square (NRMS) spectral error between data and SOMSpec prediction corresponds to the spectrum of the folded parts or populations of the peptide. This sometimes requires visual assessment of the fits. We then regenerated the percentage of α-helix and β-sheet in the original spectrum by adding back the removed random coil content.

Fluorescence studies

All buffer solutions and peptides stock solutions and solutions were prepared identically to those previously reported by us.^[13c]

Fluorescence Studies: Thioflavin T (ThT) was dissolved in water to obtain a 1.0 mM stock solution, which was protected from light and stored at -20 °C. For ThT kinetic assay studies, black polystyrene 96-well microplates with bottom optic, non-binding surfaces from Greiner Bio-One (Germany) were used. Fluorescence was measured using a CLARIOstar plate reader (BMG Labtech, Germany) with excitation and emission wavelengths of 440 and 480 nm, respectively. All experiments were performed at 37 °C under quiescent conditions. Measurements were recorded every ten minutes for the duration of the experiment. For concentration dependent studies, aliquots of peptide stock and water were added to a non-binding Eppendorf together with 10 µL 1 mM ThT. This solution was vortexed immediately prior to transfer of 135 µL into a well. Measurements were done in triplicate. The microplate was sealed using a ThinSeal™ adhesive film (Astral Scientific, Australia) to prevent sample evaporation. Fluorescence intensity was measured at regular intervals and left idle at 37 °C between measurements. After measurements in water were completed, the adhesive film was temporarily removed to allow for addition of 15 µL PBS into each well to initiate peptide aggregation.

Data processing: Baselines were measured in water or PBS and removed from the data using MARS data analysis software (BMG, Labtech) and the average of the data from the triplicates analysed using GraphPad PRISM 7 software. Data are presented with error bars for select time points and showing the sigmoidal curve of best fit as determined by the GraphPad non-linear regression analysis.

NMR spectroscopy

For NMR spectroscopy, 1.0 mg U3.5 wt was dissolved in 0.5 ml 90% H₂O/10% D₂O and pH adjusted to 5.25. Data including 2D TOCSY and NOESY (mixing time 150 ms) were recorded at 298 K and 600 MHz on a Bruker Avance III spectrometer equipped with a cryoprobe. For studies in micelles 16 mg of fully deuterated SDS was added to a final concentration of 100 mM and pH was adjusted back to 5.25. Data sets recorded at 298 K on this sample included TOCSY and NOESY (mixing time 150 ms), as well as natural abundance ¹³C and ¹⁵N HSQCs. All data were processed in Topspin 3.5 (Bruker) and analysed in CARA^[25]. Spectra were referenced to the solvent signal at 4.76 ppm.

NMR Structure Determination: NMR assignments were achieved using standard 2D sequential assignment strategies. ¹³C and ¹⁵N chemical shifts were assigned based on the ¹H chemical shifts and a TALOS-N analysis was done to generate backbone dihedral angle restraints. Structures were calculated with torsion angle dynamics within CYANA using automated assignments of NOESY data. From the final round the 20 models with the lowest CYANA^[26] target function were chosen as representative of the U3.5 wt structure in SDS micelles. Structural quality was evaluated using MOLPROBITY. The U3.5 wt NMR structure and chemical shift data have been submitted to the PDB and BMRB databases and given the access codes 7S3E and 30945, respectively.

Attenuated total reflectance Fourier transform infrared (ATR-FTIR)

Two sets of U3.x peptides and their variants were prepared in ultrapure water and 0.10 M NaCl added to reach a final concentration as 250 µM. This higher concentration than used for other measurements was to ensure sufficient fibril mass for these measurements. All the peptide samples were initially incubated at 37 °C for 48 hours then divided into two sets. After 48 hours of incubation, SDS was added to one set of peptides, to a final concentration of 10 mM SDS in the sample. This set of SDS treated peptides were incubated at 37 °C for a further 3 hours. Typical experimental method following incubation was to centrifuge the sample for ~3 minutes to concentrate the fibril mass, removal of the supernatant leaving ~50 µL that was vortexed for ~30 seconds to homogenise the mixture. The same procedure was followed for the SDS treated samples following the additional 3 hours incubation. Vibrational spectra were obtained using a FTIR ALPHA spectrometer from Bruker (Ettlingen, Germany) was used to acquire the spectra. Each sample was measured sequentially, with 5 µL deposited on the diamond crystal surface and gently dried with a stream of warm air to a dry film. All samples were measured over the wavelength range 4000–800 cm⁻¹ with a spectra resolution of 8.0 cm⁻¹ and averaged over 64 scans. All measurements were in triplicate and baselines subtracted from the peptide samples. The spectrometer was controlled using OPUS software from Bruker (Ettlingen, Germany) and converted to text format using MATLAB and plotted using GraphPad Prism. All of the data were normalized to 1.0 based on the amplitude of the amide I band observed for U3.4 wt sample.

Transmission electron microscopy

The peptides were made up to a concentration of 0.1 mg/mL in PBS solution and incubated at 37 °C for 24 hours and later stored at -20 °C. Carbon coated, 200 copper mesh grids (Proscitech, Queensland, Australia) were treated using a Gatan Solarus model 950 Advanced Plasma System (California, USA). For sample preparation, peptides were thawed to room temperature and vortexed. A 4.0 µL droplet of peptide solution was placed directly onto a plasma treated carbon disc and left to dry for 10 minutes, followed by one minute under a gentle stream of N2 gas. 4 µL of water was pipetted onto the disc and blotted off after 10 seconds. The disc was stained using a 4 µL of 2% uranyl acetate to enhance the image of the microscopic fibrils. After one-minute, filter paper was used to gently blot away excess uranyl acetate. Images were taken using a FEI Tecnai G2 T20 Twin TEM and a FEI Tecnai G2 F20 S-Twin TEM (Hillsboro, Oregon, USA) at 200 kV using Gatan CCD cameras (Gatan, California, USA).

Simulation Methods

Simulation parameters

Interactions between U3.x (wt and R/K7A) peptides with SDS micelles were simulated by performing fully-atomistic (FA) MD simulations in NAMD.^[27] The CHARMM36m force field for protein, lipid, and TIP3P water was used for modelling all inter-atomic potentials. Orthogonal simulation boxes with periodic boundary conditions applied along all three orthonormal directions were utilized for the simulations. Long-range electrostatic interactions were evaluated using the particle-mesh Ewald summation method with a grid spacing of 1 Å. A switching function was used between 10 Å and 12 Å to allow for the Lennard-Jones interactions to smoothly decay to zero. A Langevin thermostat and a Nosé-Hoover Langevin piston were applied to maintain temperature and pressure in the simulations, respectively. All simulations were carried out under physiological conditions with $T=310\text{ K}$ and a NaCl concentration of 0.15 M using an integration timestep of 2 fs. The peptide was initially kept under harmonic constraints of $10\text{ kcal mol}^{-1}\text{ Å}^{-2}$ to allow for solvent molecules to relax around the peptide. These restraints were gradually removed over a period of 2 ns. Thereafter, the simulation system was further minimized for 400 ps without any constraints. Further, equilibration was performed for 1 ns in a NVT ensemble ($T=310\text{ K}$), followed by a final equilibration run of 1 ns in a NPT ensemble ($P=1\text{ atm}$ and $T=310\text{ K}$). All systems were equilibrated with this protocol and were subsequently simulated in NPT ensembles at $P=1\text{ atm}$ and $T=310\text{ K}$ for generating production run data.

Broadly, two categories of simulations were carried out; the first involving the attachment of peptide monomers and dimers to SDS micelles, and the second involving interactions of attached peptides (in an all α -helical conformation) with SDS micelles (see Table 1). Steered molecular dynamics simulations were also performed for some of the single peptide simulations using a constant velocity of $6\times10^{-7}\text{ Å}$ per time step and a harmonic constraint spring constant of 7 kcal/mol-Å^2 . The U3.x peptide acquires a random coil structure in pure water, β -sheet rich aggregate in saline buffer and helical structure in membrane mimetic environments.^[4a,13a,c,14,24] Initial configurations of peptide monomers or dimers comprising a dominant secondary structure component (random coil, β -sheets or helices) were extracted from 1–2 µs long trajectories from simulations of either a single U3.5 wt or U3.5 R7A or multiple U3.5 wt or U3.5 R7A peptides at $T=310\text{ K}$ and 0.15 M NaCl concentration. Note: the higher concentration of NaCl used in the simulation is consistent with our first study.^[24] The

C-terminal of U3.5 wt or U3.5 R7A peptides is found to be amidated so the model peptides were amidated at C-terminal. The structure for the SDS micelle was generated with 60 SDS molecules and an approximate equilibrium diameter of 40 Å.^[28] This is very close the widely known values for SDS micelles.^[29] The SDS micelle was always placed in the centre of the simulation box and its centre of mass was constrained by harmonic constraints to stay there throughout the simulation.

Solvent-accessible surface area (SASA) could be defined as the peptide surface area accessed by a rolling sphere-probe of radius 1.4 Å, representing the aqueous solvent environment. The search parameters could be tuned to exclude solvent-interaction with the remaining peptide when calculating the SASA value for a particular peptide residue. Whereas relatively higher SASA values indicate greater solvent interaction, lower SASA values correspond to greater micellar interactions.

Acknowledgements

The authors would like to thank Dr Timothy Williams for his help obtaining TEM images and Mr John Adegoke for assistance with the ATR-FTIR measurements. We acknowledge the award of a grant from the Department of Biotechnology, Ministry of Science and Technology, India for funding support, and the SpaceTime supercomputing facility at IIT Bombay. The award of PhD stipends to AKP, CT and SR and financial support from IITB-Monash Research Academy to LLM and ASP is gratefully acknowledged.

Conflict of Interest

The authors declare no conflict of interest.

Keywords: antimicrobial peptide • amyloid • sodium dodecyl sulfate (SDS) micelle • secondary structure

- [1] R. J. Dubos, *J. Exp. Med.* **1939**, *70*, 1–10.
- [2] a) H. G. Boman, *Annu. Rev. Immunol.* **1995**, *13*, 61–92; b) K. A. Brogden, *Nat. Rev. Microbiol.* **2005**, *3*, 238–250; c) G. Diamond, N. Beckloff, A. Weinberg, K. O. Kisich, *Curr. Pharm. Des.* **2009**, *15*, 2377–2392; d) J. Vizioli, M. Salzet, *Trends Pharmacol. Sci.* **2002**, *23*, 494–496.
- [3] a) V. Baltutis, A. N. Calabrese, J. A. Carver, L. L. Martin, in *Antimicrobial Peptides: Function, Mechanisms of Action and Role in Health and Disease* (Ed.: P. C. Ray), Nova Science Publishers, 2021; b) A. H. Benfield, S. T. Henriques, *Front. Med. Technol.* **2020**, *2*, 610997. doi: 10.3389/fmedt.2020.610997.
- [4] a) A. N. Calabrese, Y. Liu, T. Wang, I. F. Musgrave, T. L. Pukala, R. F. Tabor, L. L. Martin, J. A. Carver, J. H. Bowie, *ChemBioChem* **2016**, *17*, 239–246; b) A. Izadpanah, R. L. Gallo, J. Am. Acad. Dermatol. **2005**, *52*, 381–390; c) A. K. Mahalka, P. K. J. Kinnunen, *Biochim. Biophys. Acta Biomembr.* **2009**, *1788*, 1600–1609.
- [5] a) C. Auvinet, C. El Amri, C. Lacombe, F. Bruston, J. Bourdais, P. Nicolas, Y. Rosenstein, *FEBS J.* **2008**, *275*, 4134–4151; b) L. Caillon, J. A. Killian, O. Lequin, L. Khemtémourian, *PLoS One* **2013**, *8*, e75528; c) H. Chu, M. Pazgier, G. Jung, S.-P. Nuccio, P. A. Castillo, M. F. de Jong, M. G. Winter, S. E. Winter, J. Wehkamp, B. Shen, N. H. Salzman, M. A. Underwood, R. M. Tsolis, G. M. Young, W. Lu, R. I. Lehrer, A. J. Bäumler, C. L. Bevins, *Science* **2012**, *337*, 477; d) Y. A. Domanov, P. K. Kinnunen, *Biophys. J.* **2006**, *91*, 4427–4439; e) H. Jang, F. T. Arce, M. Mustata, S. Ramachandran, R. Capone, R. Nussinov, R. Lal, *Biophys. J.* **2011**, *100*, 1775–1783; f) B. L. Kagan, H. Jang, R. Capone, F. Teran Arce, S. Ramachandran, R. Lal, R. Nussinov, *Mol. Pharmaceutics* **2012**, *9*, 708–717; g) L. Schnaider, S.

- Brahmachari, N. W. Schmidt, B. Mensa, S. Shaham-Niv, D. Bychenko, L. Adler-Abramovich, L. J. W. Shimon, S. Kolesheva, W. F. DeGrado, E. Gazit, *Nat. Commun.* **2017**, *8*, 1365; h) X. Tian, F. Sun, X.-R. Zhou, S.-Z. Luo, L. Chen, *J. Pept. Sci.* **2015**, *21*, 530–539; i) M. Zhang, J. Zhao, J. Zheng, *Soft Matter* **2014**, *10*, 7425–7451; j) H. Zhao, A. Jutila, T. Nurminen, S. A. Wickström, J. Keski-Oja, P. K. J. Kinnunen, *Biochemistry* **2005**, *44*, 2857–2863; k) H. Zhao, R. Sood, A. Jutila, S. Bose, G. Fimland, J. Nissen-Meyer, P. K. J. Kinnunen, *Biochim. Biophys. Acta Biomembr.* **2006**, *1758*, 1461–1474.
- [6] a) E. Y. Lee, Y. Srinivasan, J. de Anda, L. K. Nicastro, Ç. Tükel, G. C. L. Wong, *Front. Immunol.* **2020**, *11*; b) M. Torrent, J. Valle, M. V. Nogués, E. Boix, D. Andreu, *Angew. Chem. Int. Ed. Engl.* **2011**, *50*, 10686–10689.
- [7] a) F. Harris, S. R. Dennison, D. A. Phoenix, *FASEB J.* **2012**, *26*, 1776–1781; b) R. D. Moir, R. Lathe, R. E. Tanzi, *Alzheimers Dement.* **2018**, *14*, 1602–1614.
- [8] a) R. M. Epand, R. F. Epand, *Biochim. Biophys. Acta Biomembr.* **2009**, *1788*, 289–294; b) N. Papo, Y. Shai, *Cell. Mol. Life Sci.* **2005**, *62*, 784–790.
- [9] N. B. Last, A. D. Miranker, *PNAS* **2013**, *110*, 6382.
- [10] a) M. A. Apponyi, T. L. Lukala, C. S. Brinkworth, V. M. Maselli, J. H. Bowie, M. J. Tyler, G. W. Booker, J. C. Wallace, J. A. Carver, F. Separovic, J. Doyle, L. E. Llewellyn, *Peptides* **2004**, *25*, 1035–1054; b) J. H. Bowie, F. Separovic, M. J. Tyler, *Peptides* **2012**, *37*, 174–188; c) A. Bradford, M. Raftery, J. Bowie, M. Tyler, J. Wallace, G. Adams, C. Severini, *Aust. J. Chem.* **1996**, *49*, 475–484; d) A. M. Bradford, J. H. Bowie, M. J. Tyler, J. C. Wallace, *Aust. J. Chem.* **1996**, *49*, 1325–1331.
- [11] B. C. S. Chia, J. H. Bowie, J. A. Carver, T. D. Mulhern, *J. Pept. Res.* **1999**, *54*, 137–145.
- [12] T. J. Falla, D. N. Karunaratne, R. E. W. Hancock, *J. Biol. Chem.* **1996**, *271*, 19298–19303.
- [13] a) T. John, T. J. A. Dealey, N. P. Gray, N. A. Patil, M. A. Hossain, B. Abel, J. A. Carver, Y. Hong, L. L. Martin, *Biochemistry* **2019**, *58*, 3656–3668; b) L. L. Martin, C. Kubeil, S. Piantavigna, T. Tikkoo, N. P. Gray, T. John, A. N. Calabrese, Y. Liu, Y. Hong, M. A. Hossain, N. Patil, B. Abel, R. Hoffmann, J. H. Bowie, J. A. Carver, *Pept. Sci.* **2018**, *110*, e24052; c) S. Ray, S. Holden, A. K. Prasad, L. L. Martin, A. S. Panwar, *J. Phys. Chem. B* **2020**, *124*, 11659–11670.
- [14] N. Salinas, E. Tayeb-Fligelman, M. D. Sammito, D. Bloch, R. Jelinek, D. Noy, I. Usón, M. Landau, *PNAS* **2021**, *118*, e2014442118.
- [15] J. H. Bowie, F. Separovic, M. J. Tyler, *Peptides* **2012**, *37*, 174–188.
- [16] D. E. Otzen, *Curr. Protein Pept. Sci.* **2010**, *11*, 355–371.
- [17] C. I. Schroeder, K. J. Rosengren, in *Snake and Spider Toxins: Methods and Protocols* (Ed.: A. Priel), Springer US, New York, NY, **2020**, pp. 129–162.
- [18] D. S. Wishart, C. G. Bigam, A. Holm, R. S. Hodges, B. D. Sykes, *J. Biomol. NMR* **1995**, *5*, 67–81.
- [19] Y. Shen, A. Bax, *J. Biomol. NMR* **2013**, *56*, 227–241.
- [20] a) V. Hall, M. Sklepari, A. Rodger, *Chirality* **2014**, *26*, 471–482; b) A. Olamoyesan, D. Ang, A. Rodger, *RSC Adv.* **2021**, *11*, 23985–23991.
- [21] L. S. Wolfe, M. F. Calabrese, A. Nath, D. V. Blaho, A. D. Miranker, Y. Xiong, *PNAS* **2010**, *107*, 16863–16868.
- [22] K. Yamaguchi, H. Naiki, Y. Goto, *J. Mol. Biol.* **2006**, *363*, 279–288.
- [23] a) R. Sarroukh, E. Goormaghtigh, J.-M. Ruyschaert, V. Raussens, *Biochim. Biophys. Acta Biomembr.* **2013**, *1828*, 2328–2338; b) J. Waeytens, V. Van Hemelryck, A. Deniset-Besseau, J.-M. Ruyschaert, A. Dazzi, V. Raussens, *Molecules* **2020**, *25*, 2899.
- [24] S. Ray, S. Holden, L. L. Martin, A. S. Panwar, *Pept. Sci.* **2019**, *111*, e24120.
- [25] R. L. J. Keller, *The computer aided resonance assignment tutorial*, **2004**, CANTINA Verlag.
- [26] P. Güntert, *Methods Mol. Biol.* **2004**, *278*, 353–378.
- [27] J. C. Phillips, R. Braun, W. Wang, J. Gumbart, E. Tajkhorshid, E. Villa, C. Chipot, R. D. Skeel, L. Kalé, K. Schulten, *J. Comput. Chem.* **2005**, *26*, 1781–1802.
- [28] A. D. MacKerell, *J. Phys. Chem.* **1995**, *99*, 1846–1855.
- [29] S. Hayashi, S. Ikeda, *J. Phys. Chem.* **1980**, *84*, 744–751.
- [30] A. Waterhouse, M. Bertoni, S. Biener, et al., *Nucleic Acids Research* **2018**, *46* (W1), W296–W303.
- [31] J. P. F. Strumpfer, C. Chipot, *Molefacture: A tutorial to build and edit molecules*. Centre National de la Recherche Scientifique, University of Illinois, Urbana – Champaign c) <http://www.ks.uiuc.edu/Research/vmd>, 2012.
- [32] W. Humphrey, A. Dalke, K. Schulten, *J. Mol. Graph.* **1996**, *14* (1), 33–38.

Manuscript received: September 8, 2021

Revised manuscript received: November 10, 2021